IEEE Access
Multidisciplinary | Rapid Review | Open Access Journal

Received June 27, 2021, accepted July 18, 2021, date of publication July 21, 2021, date of current version July 28, 2021.

Digital Object Identifier 10.1109/ACCESS.2021.3098983

Dual-Polarized Wide-Angle Energy Harvester for Self-Powered IoT Devices

MINH DINH[1], (Member, IEEE), NAM HA-VAN[2], (Member, IEEE), NGUYEN THANH TUNG[3], (Member, IEEE), AND MINH THUY LE[1], (Member, IEEE)

[1]School of Electrical Engineering, Hanoi University of Science and Technology, Hanoi 10000, Vietnam
[2]Department of Electronics and Nanoengineering, Aalto University, 02150 Espoo, Finland
[3]Institute of Materials Science, Vietnam Academy of Science and Technology, Hanoi 10000, Vietnam

Corresponding author: Minh Thuy Le (thuy.leminh@hust.edu.vn)

This work was funded by Vingroup Joint Stock Company (Vingroup JSC), Vingroup and supported by Vingroup Innovation Foundation (VINIF) under project code VINIF.2020.DA09.

ABSTRACT In this work, a dual-polarized wide-angle energy harvester operating at 3.75 GHz is proposed for ambient RF energy harvesting applications. A 4 × 4 array harvester can efficiently harvest incident RF waves from all polarizations, resulting in high RF-AC efficiency of 94% and final RF-DC efficiency of 34% at 0.02 W/m^2 input power density, or −15 dBm input power. This performance is preserved under a wide incident angle up to 65 degrees in TE mode and 75 degrees in TM mode. Owing to its simple power combining configuration, the array can be easily expanded to incorporate more unit cells, increasing the amount of collected power. Not only having the RF-DC conversion function, it is also equipped with a power management circuit to create a usable output voltage level. With this advantage, the harvester is suitable to be employed in real-life applications in which the polarization and angle of incidence are unknown and the incident power is very low.

INDEX TERMS Dual-polarization, self-powered IoT device, metamaterial absorber, rectennas, RF energy harvesting.

I. INTRODUCTION

Metamaterial absorber (MMA) has been first introduced by Landy *et al*. [1]. Many efforts have been spent to exploit its unnatural property, which fully absorbs incident electromagnetic waves at a desired range of frequencies. In most applications of MMAs, such as reducing radar cross-section [2] or sensing [3], etc., a large amount of the absorbed power is wasted in the form of heat loss. Most earlier works on the MMAs only focused on the absorbing aspect without examining what happens after absorption. The electromagnetic energy harvester is one of the potential uses of MMAs that the absorbed power is transformed into a usable one. Instead of being dissipated away, a major part of the absorbed power can be rectified into DC before being transferred to a consuming device. This provides a solution to the traditionally unused power in MMAs. The application of MMAs on energy harvesting became even more promising and prominent as the recent advances in semiconductor technology give rise to electronic devices with very low power consumption, wireless sensors, for example, only consume several nW in sleep mode, several mWs in core active mode and around 10 to 30 mW in full active, transmitting, and receiving mode [4], [5]. Using MMAs for energy harvesting, especially at RF frequencies, also brings various benefits. The most evident one is that its high absorptance promises a good RF – AC efficiency. Besides, MMAs can be easily arrayed to extend the surface area to collects more ambient power. These properties are crucial in real-life condition, where the RF sources, such as GSM, Wi-Fi, 3G, or 4G, may be available and ubiquitous but yield a very low power density, usually lower than 1 μW/cm^2 (or 0.01 W/m^2) [6], [7], and vary in different locations. Therefore, to harvest enough power, sometimes up to dozens of mW, expanding the surface area to receive more incident waves is inevitable, and MMA is a suitable candidate.

One of the pioneer's works in MMAs for energy harvesting is from Almoneef and Ramahi [8], in which an array of split–ring resonators achieved a high RF–AC conversion

The associate editor coordinating the review of this manuscript and approving it for publication was Raghvendra Kumar Chaudhary.

efficiency of 96%. A near-unity RF–AC efficiency was also witnessed in [9] and [10] in where the omega–ring and the complement quad split–ring are employed. These works, however, only investigated the RF–AC conversion stage while the indispensable rectifier was replaced with an equivalent resistor. The structure in [8] and [9] are also asymmetric and therefore unable to harvest RF waves of all polarizations. Only a few works of literature have comprehensively examined the full metamaterial absorber–based energy harvester, from the RF power collecting to rectification, notably [11] and [12]. However, both of them, despite having very high efficiency, nearly 70%, were tested under input power higher than 0 dBm, which rarely happens in practical conditions. The harvester in [11] also employs the angle–sensitive RF–combine configuration, which makes it practically unsuitable, while the harvester in [12] has its angle dependency unexamined. Another crucial part of an energy harvesting system is the power management circuit that is usually overlooked and replaced with an equivalent resistor in most previous works. In reality, the consuming devices firstly require a certain voltage level, for instance from 1.8 VDC to 5 VDC, that usually exceeds the supply by a typical rectenna under a low input power. Besides, in practical conditions, incident power density varies continuously leading to a non-constant output voltage of the rectenna. Therefore, a power management circuit is necessary to overcome these problems that can provide a suitable output to sustain the devices.

In this work, an MMA harvester is proposed with high RF-DC efficiency at low input power for all polarizations. In addition, an effective DC-combiner is configured that can maintain the performance under a wide incident power angle. The simplicity of the design allows it to be easily expanded to incorporate more unit cells with minor modifications. Furthermore, the harvester is equipped with a power management circuit that effectively produces a suitable DC output voltage of 3.3 V. Finally, the proposed energy harvester is suitable to be applied in practical applications, being the power supply of low–powered wireless devices with high conversion efficiency at low incident power, incident angle insensitivity, and power management integration.

II. METAMATERIAL HARVESTER UNIT CELL DESIGN

A. METAMATERIAL ABSORBER UNIT CELL DESIGN

The proposed MMA is designed to operate at 3.75 GHz frequency that is a periodic array of identical unit cells. Each unit cell consists of five layers as shown in Fig. 1. The symmetrical cross – shaped resonator is placed on top of a dielectric substrate, followed by a ground plane with two aperture slots to transfer the collected power. Two feeding lines and rectifiers are designated at the bottom of another dielectric substrate. The materials for the first and second substrate are RT Duroid5880 ($\varepsilon_1 = 2.2$, $\tan\delta_1 = 0.0009$) and Rogers RO4003C ($\varepsilon_2 = 3.55$, $\tan\delta_2 = 0.0027$), respectively. The dimensional parameters are $p = 40$ mm, $l = 27$ mm, $w = 12$ mm, $l_a = 9$ mm, $a = 8$ mm, $w_a = 1.5$ mm,

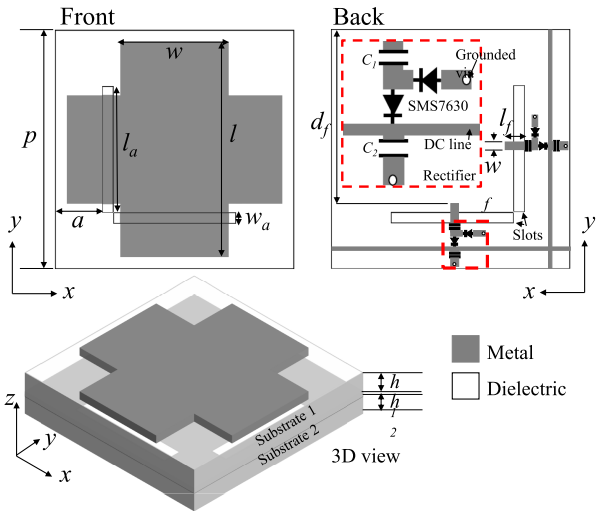

FIGURE 1. 3D structure of the unit cell.

$d_f = 24.5$ mm, $l_f = 8$ mm, $w_f = 1$ mm, $w_{DC} = 0.5$ mm, $h_1 = 2.54$ mm and $h_2 = 0.8$ mm.

The operating principle of the MMA can be explained by the equivalent circuit and impedance matching theory. When incident waves approach the MMA, the external magnetic fields flowing through the gap between the cross resonator and the ground plane induce an anti-parallel current running on their surfaces, as shown in Fig. 2(a). This current in turn creates a secondary magnetic field against the external one that can be considered to an equivalent inductor L. The near–field electric fields concentrate mostly on the two edges of the resonator to form an equivalent capacitor C. Since the conductive material is non–ideal, a serial resistor R_C is added next to the inductor to represent the ohmic loss. Another resistor R_R represents the feeding lines and rectifiers that is placed at the end of a 377 Ω transmission line representing free–space, as shown in Fig. 2(b). Normally, the near–field electric fields are not just located between the resonator and the ground but parts of them "flow" from one cell to the next one. This coupling electric fields form another equivalent capacitor [13], which represents the mutual coupling between adjacent unit cells. By giving p a sufficiently large value, the cells are placed far enough from each other, thus, this equivalent capacitance can be negligible.

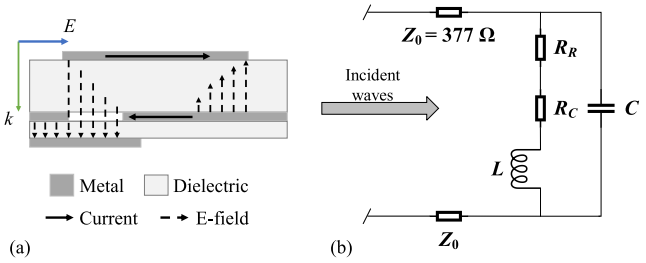

FIGURE 2. (a) Simplified currents and *E*-field distribution in the unit cell, (b) equivalent circuit of the structure.

From the equivalent circuit model, the MMA's input impedance Z_{in} can be easily derived as

$$Z_{in} = \frac{i/2C}{2\pi(f - f_o) + i(R_C + R_R)/2L} \quad (1)$$

where f and f_o are the frequency of incident waves and the resonant frequency of the MMA, respectively. Here we only investigate the frequency range $f \simeq f_o$ and assume that the damping factor $(R_C + R_R)/2L \ll 2\pi f$ (high quality resonance). Perfect absorption at $f = f_o$ is achieved if $Z_{in}(f_o) = Z_o = 377\ \Omega$. From (1), the condition for perfect absorption can be obtained by

$$\frac{1}{(R_C + R_R)LZ_o} = 1 \quad (2)$$

The inductance, capacitance and resistance of two parallel metallic plates can be expressed as

$$L = \frac{\mu h_1 l}{w}, \quad C = \frac{\varepsilon w l}{h_1}, \quad R = \frac{1}{\sigma w \delta} \quad (3)$$

where μ is the free–space permeability, σ is the conductivity, and δ is the skin–depth. The resonant frequency f_o primarily depends on l, which is the first parameter to be determined in order to achieve a resonant frequency of 3.75 GHz. With l being fixed, other parameters, namely w, w_f, d_f, l_f, etc, are optimized to achieve suitable values for R_R, R_C to satisfy (2), and obtain the perfect absorption. In ideal case, the metal is perfectly conductive conducive to $R_C = 0$. However, metallic loss is always exists as an undesired effect. Therefore, the incident waves being admitted to the MMA will be consumed by R_C and R_R, the value of R_R has to be considerably larger than R_C. The larger R_R is compared to R_C, the more power delivered to the rectifiers.

The unit cells, due to their symmetry, provide the same response for all polarizations. The vertically and horizontally polarized waves are respectively absorbed by each ''arm'' of the cross and harvested by the corresponding rectifier. The cross-shaped MMA has been proven to be angle-insensitive in [14], [15] with the absorptance maintained higher than 80% under 60° incident angle in TE mode, and higher than 90% under 70° incident angles in TM mode. In TE mode, when the incident angle increases, the portion of the magnetic field that flows through the gap between the resonator and the ground plane is decreased leading to the weaker induced current. While the magnetic flux in TM mode remains stable no matter how wide the incident angle is, however, the resonant frequency is gradually shifted away. This frequency shift can be attributed to the portion of the external electric field perpendicular to the ground plane, which gets stronger as the angle increases and causes changes in the E–field distribution between the resonator and the ground thus changes the equivalent capacitance. To the best of our knowledge, a comprehensive and exact mathematical description for the behavior of the cross-shaped MMAs or angle-insensitive MMAs, in general, has not been presented yet. In our design process, we use a quantitative approximation drawn from the Fresnel equations when consider the entire metamaterial absorber equivalent to a homogeneous dielectric slab of effective permittivity $\varepsilon = 2.2$, permeability $\mu = 1$ and refractive index $n = \sqrt{\mu\varepsilon}$. The reflection coefficient in the TE and TM mode at an incident angle θ is calculated by

$$\gamma_{TE}(\theta) = \frac{cos\theta - \sqrt{n^2 - sin^2\theta}}{cos\theta + \sqrt{n^2 - sin^2\theta}} \quad (4)$$

$$\gamma_{TM}(\theta) = \frac{-n^2 cos\theta - \sqrt{n^2 - sin^2\theta}}{n^2 cos\theta + \sqrt{n^2 - sin^2\theta}} \quad (5)$$

Since the MMA is terminated with a metallic ground plane, no transmission is allowed at all. The absorptance A and the RF–AC efficiency η_{RF-AC} are therefore calculated from the simulated S– parameters as following

$$A = 1 - |S_{Zmax,Zmax}|^2 = 1 - |\gamma|^2 \quad (6)$$

$$\eta_{RF-AC} = |S_{1,Zmax}|^2 + |S_{2,Zmax}|^2 \quad (7)$$

The absorptance, with an incident angle less than 60°, calculated using (4), (5), and (6) is 85% and 90% in the TE and TM mode, respectively. This calculation is not perfectly accurate because the effective permittivity and permeability may slightly change their values due to the impact of resonance [16]. Nevertheless, since promising results have been achieved before with the same cross–shaped structure, a comparable performance can be expected for this harvester.

The electromagnetic properties of MMA are simulated using the finite integration technique embedded in the CST software. The boundary condition is set to ''unit cell'', the incident power is excited by the Floquet port Z_{max}. For the sake of simplicity, the two rectifiers are replaced by two lumped ports with the same input impedance of 50 Ω. It is worth noticing that the impedance of the rectifiers does not have to be exact 50 Ω, it just has to match with the MMA impedance seen from the ports. However, both the MMA and the rectifiers are designed with their input impedances to equal 50 Ω so that the rectifier can be easily connected with network analyzers or spectrum analyzers for testing.

Simulation results are shown in Fig. 3(a). The metamaterial absorber achieves a maximum absorptance and RF–AC efficiency of 97% and 94% under normal incidence respectively and maintains them higher than 60% with incident angle as wide as 70° in the TE mode. Meanwhile, in the TM mode, as the incident angle increases up to 70°, the efficiency stills remain around 80%. In the experiment, two identical linearly-polarized antennas are connected to a signal generator and a spectrum analyzer, and placed at 1.5 m away from the MMA, at α and $-\alpha$ angle. A calibration step is first performed with a plain copper sheet to achieve the received power P_{cal} correspond with 100% reflection. Two antennas are rotated around the MMA to vary the incident angle from 0% to 90% at TE and TM mode, respectively. The received power at the spectrum analyzer P_r is used to calculate the absorptance A

$$A = \frac{P_{cal} - P_r}{P_{cal}} \quad (8)$$

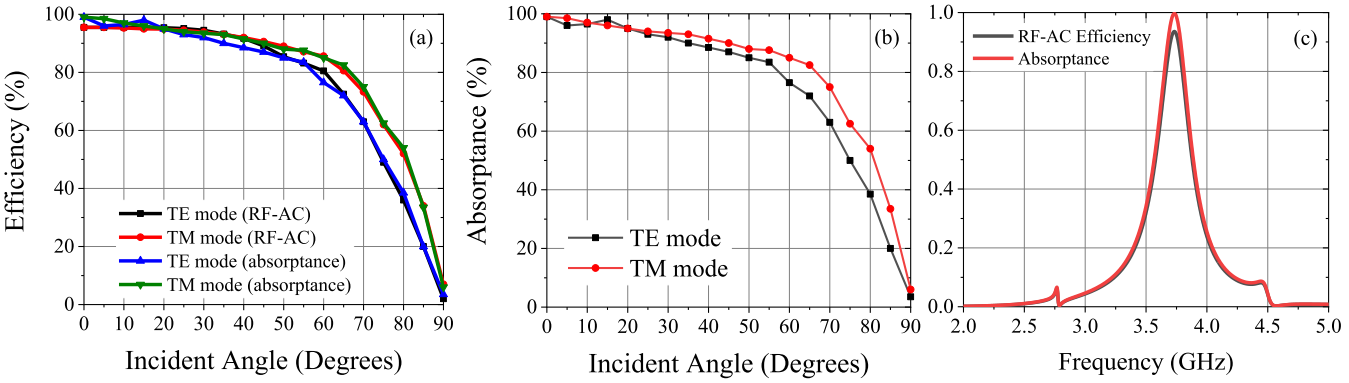

FIGURE 3. (a) Simulated absorptance and RF-AC efficiency of the MMA as a function of incident angle; (b) measured absorptance of the MMA as a function of incident angle; (c) simulated absorptance and RF-AC efficiency spectra under normal incidence.

The measured absorptances have a good agreement with the simulation, as shown in Fig. 3(b), that provide the wide–angle property of the MMA. The simulated absorptance and RF-AC efficiency spectra of the harvester is shown in Fig. 3(c).

B. RECTIFIER AND DC POWER COMBINER DESIGN

For metamaterial harvester or rectenna arrays in general, there are two ways of combining the harvested power: RF–combiner, and DC–combiner. The RF-combiner gives higher efficiency under normal incidence. However, this topology can only maintain the performance at a very narrow-angle, and unsuitable for practical situations. The main reason for the angle dependency is the phase mismatches between the unit cells (or antenna elements). The cells may be in – phase with each other under normal incidence, but only a small angle deviation is needed for them to be out – of – phase. Their collected power then cancels each other, decreasing the RF – AC efficiency considerably, even if the absorptance remains high. This can be seen in normal antenna arrays, where more antenna elements incorporated results in narrower beamwidth. The same is applied with MMAs. A wide–angle absorption alone is therefore not enough but also a suitable power combining method is needed as well. The second method, rectify the collected power in each cell before combining them, is more favorable since the combining step is taken when they are already DC. However, by using the DC-combined configuration, a unique challenge arises: because each unit cell is equipped with its rectifiers, the rectifiers will have to be compact enough to stay fit within a small area of the cell. This requirement will be addressed below. As shown in Fig. 1, each unit cell is equipped with two voltage doubler rectifiers. The SMS 7630 Schottky diode is chosen due to its good performance at low input power [17] while the two capacitors have the same value of 470 pF. To satisfy the requirement of compactness, the commonly seen impedance matching stubs are not employed to match the rectifier's input impedance with 50 Ω. Instead, the lengths and widths of the microstrip lines and the values of the capacitors are carefully

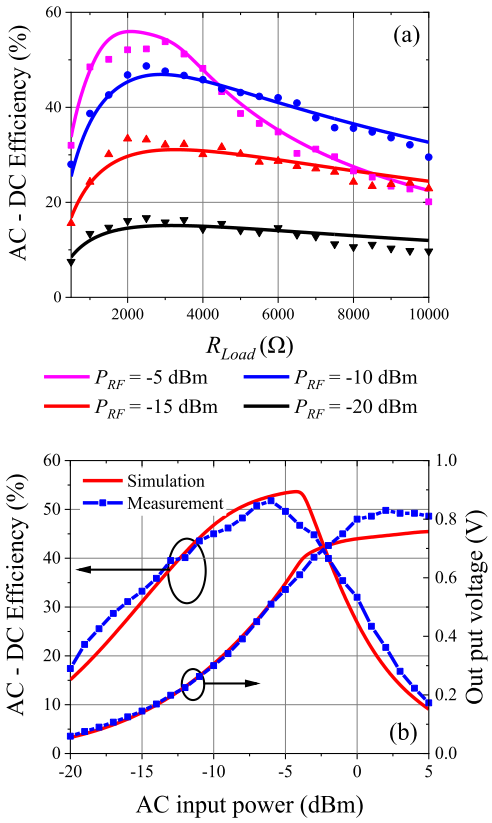

FIGURE 4. Simulated and measured AC-DC efficiency of the rectifier as a function of load (a) and input power (b).

chosen. The rectifiers of adjacent unit cells are parallelly connected via the DC combining lines in which the harvested DC power is delivered to the load. Since the combined powers are already DC, the combining lines are allowed to cross each other. Meanwhile, in the RF-combined method, the combining lines of each polarization are to be separated [11] to avoid cross-talk between them. The simplicity, therefore, becomes another key advantage of this MMA–based rectenna. In this configuration, the collected DC power of each polarization of each unit cell can only flow in one direction toward the load

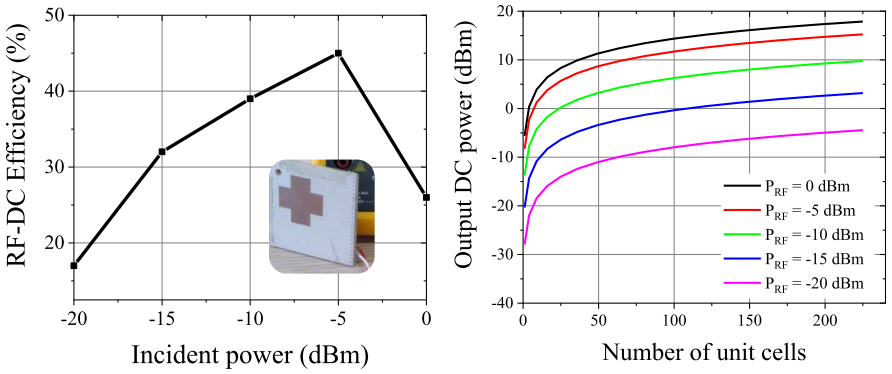

FIGURE 5. Measured unit cell's RF-DC efficiency (left), and calculated output power as a function of cells number and incident power, assuming the angle of incidence to be normal (right).

because other directions are either open-circuited or blocked by the diodes of other rectifiers.

An individual rectifier is simulated using ADS in which the feed line is modeled as an AC source having an input impedance of 50 Ω and the diodes are modeled using the SPICE model. The parasitic inductance and capacitance of the diode are also taken into account. Instead of being linked to other cells, the rectifier is terminated with a resistor to represent the optimal load of each cell. The simulation result shows a maximum AC-DC efficiency of 31.5% at −15 dBm input power and the load R_L of 3 kΩ, while in measurement, a 2 kΩ load produces the best result of 33.5%, as shown in Fig. 4(a). An AC-DC efficiency is higher than 30% in the R_L range varied from 1.8 kΩ to 6 kΩ. With the load being fixed at the optimal value of 2 kΩ, maximum AC-DC efficiency of 52%, correspond with a DC output voltage of 520 mV, was achieved at −7 dBm input power. At low input power, namely −20 dBm, −15 dBm and −10 dBm, the measured efficiency and output voltage are 18%, 33.5%, 45% and 60 mV, 151 mV, 306 mV, respectively, as shown in Fig. 4(b). It is worth noticing that since each rectifier has an optimal load value $R_L = 2\ \text{k}\omega$ and they are parallelly linked together, the optimal load of an n – cell harvester will be R_L/n. This means the more cells the harvester consists of, the smaller its optimal load becomes. And since the simple design enables the ability to easily incorporate more cells, the optimal load can be made as small as possible. The benefit of a small optimal load will be discussed in the next section. From Fig. 4(a), one may also expect the overall performance (at low input power) to be relatively stable in a wide range of load resistance, given the ''gentle'' shapes of the curves.

C. SINGLE UNIT CELL TESTING

With the unit cells being equipped with their own rectifiers and placed far enough from each other to minimized mutual coupling, the MMA is in fact an array of individual rectennas assembled together. Each one of them operates independently, with little effect from neighboring cells. The total collected power therefore can be approximated to be in proportion with the number of unit cells.

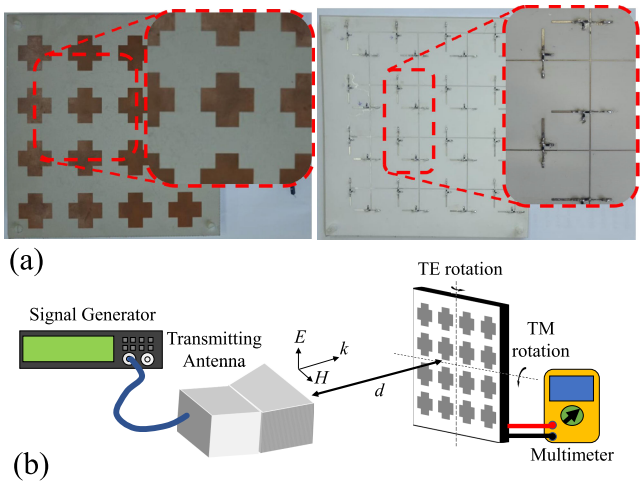

FIGURE 6. (a) Real image of the prototype harvester, (b) the harvester under measurement.

From the above results of RF-AC and AC-DC conversion stages, one may calculate or estimate the RF-DC efficiency and harvested DC power of one single unit cell, and then n-cell array using the following equation

$$P_{DC} = n\eta_{RF-AC}\eta_{AC-DC}P_{RF} \tag{9}$$

where P_{DC} is the output power, P_{RF} is the incident power, η_{RF-AC} and η_{AC-DC} are the RF–AC and AC–DC efficiency. A prototype individual unit cell is also constructed and tested under the excitation from a high gain reference antenna (the measurement setup, similar to the full array, will be described in the next section). The RF–DC efficiency fits well with the calculation. More specifically, the measured single-cell RF – DC efficiency is 26%, 45%, 39%, 32% and 17% at 0, −5, −10, −15 and −20 dBm input power, respectively, equivalent to an incident power density of 0.6, 0.2, 0.06, 0.02 and 0.006 W/m^2. From that, the number of unit cells to provide enough power for a particular consuming device can be determined. For example, assume the harvester to be used in a region where the typical value of incident power

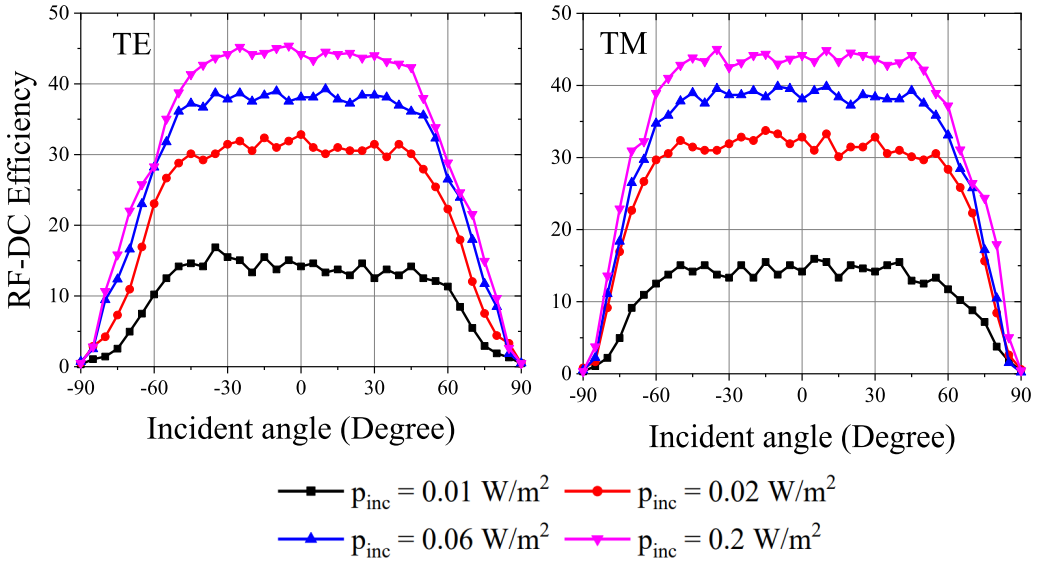

FIGURE 7. Measured RF – DC efficiency under different incident angle in TE and TM mode.

density is 0.06 W/m^2, or -10 dBm per cell, a 100 – cell array is expected to harvest up to 5 mW, as shown in Fig. 5.

III. METAMATERIAL HARVESTER TESTING

After examining the performance of an individual cell separately, as a proof of concept, a 4 × 4 harvester is fabricated and measured using the 5G trial source at the 3.75 GHz band. A 120 Ω resistor, corresponds with $n = 16$ (125 Ω to be precise, however, 120 Ω resistors are more commonly found), is connected to the harvester to represent the load.

In the measurement set–up as in Fig. 6, a linearly polarized high gain antenna excites 3.75 GHz corresponding with incident waves at different power levels. The incident power density p_{inc} is calculated after the transmitted power P, reference antenna gain G (which is 14 dBi), and distance d, which we kept at least 2 meters, between the harvester and the reference antenna:

$$p_{inc} = \frac{PG}{4\pi d^2} \tag{10}$$

Distance d and excitation power P are varied to create different levels of incident power density. At each position, the absorber is rotated around its vertical and horizontal axis in order to change the incident angle from $-90°$ to $90°$ in respective TE and TM mode. The output DC voltage V_{out} is measured and displayed on a digital multimeter, and from that, the RF–DC efficiency η_{RF-DC} is calculated as follow

$$\eta_{RF-DC} = \frac{V_{out}^2}{ARp_{inc}} 100\% \tag{11}$$

where A is the area of the harvester.

The measured RF–DC efficiency is displayed in Fig. 7. A wide–angle performance is visible. Under normal incidence, at 0.02 W/m^2 power density, correspond with an input power of -15 dBm each cell, the efficiency is 33%. Efficiency higher than the half-maximum is obtained as the incident angle varies between $\pm 65°$ in TE and $\pm 70°$ in TM mode. This means the harvester can efficiently harvest incident RF waves coming from many directions. This trait is expected since the harvested power is rectified before being combined.

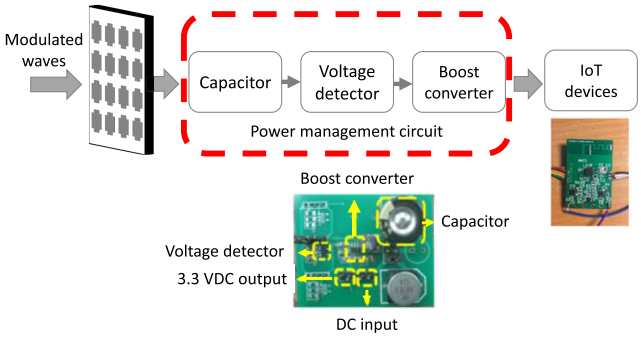

FIGURE 8. Block diagram of the harvester with power management.

From Fig. 7, one can easily calculate the amount of power harvested. For example, under a low power density of 0.01 W/m^2, the 4 × 4 array harvests 7.6 μW in total, which is still insufficient to fully sustain most low–power devices, however, it is enough for sleep mode and some limited functions. By increasing the number of unit cells, one may expect to collect enough power for a device to operate at full function. In calculation, under the same power density, a 25 × 25 array, with the size of 100 x 100 cm harvests up to 3 mW, which is sufficient for some low–powered devices, such as wireless sensor nodes in [4], [5].

IV. POWER MANAGEMENT

In addition to efficiency, the DC voltage has to meet a certain level. Therefore, a boosting circuit is indispensable.

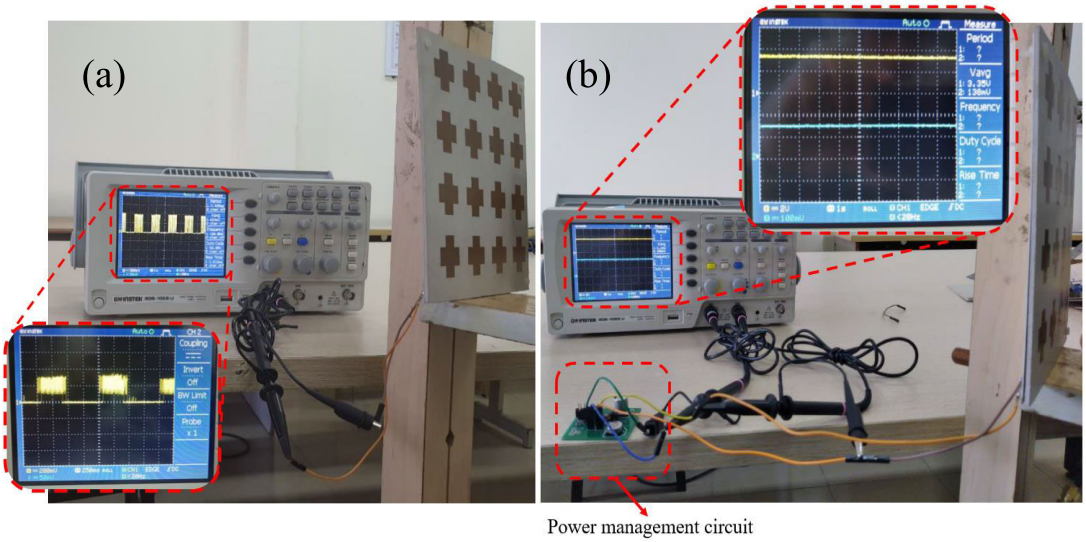

FIGURE 9. Output voltage without (a) and with (b) power management. In (b), channel 1 of the oscilloscope (yellow) shows the final boosted voltage while channel 2 (blue) shows the output voltage of the harvester.

TABLE 1. A comparison between this work and related work.

References	Frequency (GHz)	Polarization	Input power density (W/m^2)	Efficiency (%)	Load Ω	Half-efficiency Angle (Degrees)	Power Management
[12]	3	Dual	0.3	20	600	-	No
[21]	2.8	Linear	1.1	40	200	Narrow	No
[23]	3.2	Linear	0.83	40	300	-	No
[26]	0.9	Linear	3.7	15	70 to 80	-	No
[27]	2.45	Linear	5	47	400	-	No
This work	3.75	Dual	0.02	34	120	65^o (TE mode) 70^o (TM mode)	Yes

Another problem arises, in a practical situation, incident waves are often inconsistent and modulated, resulting in an unstable output voltage. For instance, the 5G broadcasting signals are repeatedly transmitted every few seconds. In this case, an intermediate capacitor is needed to stabilize the output before this voltage can be boosted. Under RF incidence, the capacitor is charged, the charging process will be halted when the incident wave is absent. During this short absence, the capacitor will not discharge due to the appearance of the diodes. Gradually, when the intermediate capacitor's voltage reaches a certain level, the voltage detector placed right behind it will open, allowing the stored power to be transferred to the boost converter.

The block diagram of the harvester with power management is shown in Fig. 8. Seen from the power management circuit, the rectenna is equivalent to a DC source with an intrinsic resistor which equal the optimal load.

The capacitor takes time to be fully charged. The time constant therefore has to be small. In order to store enough energy, the capacitance has to be large, therefore, a small source resistance is desirable. This metamaterial harvester, by parallelly connecting the rectified unit cells together, possesses a small optimal load. This property helps quickly charge the capacitor and achieve a usable output voltage.

In our measurement, the resistive load is replaced by a power management circuit. The incident wave is modulated in OFDM method and generated as intermittently to mimic practical condition. It is visible that without the power management circuit, the output is unstable, having a pulse – like waveform (due to the OFDM modulated method), while the output with power management is smooth and stable, having a sufficient value of 3.3 VDC, as shown in Fig.9.

To examine the response time of the power management circuit, modulated waves were continuously transmitted toward the harvester. With a 2.2 F supercapacitor, the amount of time until a 3.3 VDC output is generated is 5 minutes and 14 seconds. This charging time can even be made smaller by further increasing the number of unit cells. For instance, an 8×8 array, which is equivalent to a 30 Ω voltage source, is expected to reach the desired voltage 4 times faster than the prototype 4×4 harvester, only around 80 seconds. Obviously, the results of this experiment are not necessarily the ones we achieve in practical applications, since the excitation signal in the experiment was continuous, with constant magnitude.

A comparison between the harvester of this work and other works is provided in Table 1. The two main criteria to be compared are RF–DC efficiency, especially under low input power or power density, and the incident angle in which efficiency decreases by half. The structure of this work possesses a visibly wider half–power angle while having a comparable efficiency under normal incidence. It also has the smallest optimal load, which proves to be crucial later on.

V. CONCLUSION

In conclusion, we have proposed and investigated a metamaterial harvester for energy harvesting applications. By employing metamaterial and equipping each unit cell with its own rectifiers, the structure can harvest RF power in the ambient environment. The recorded RF–DC efficiency is as high as 34% under 0.02 W/m^2 power density, which is close to real life condition, and maintain that performance with wide incident angle, up to 65o and 70° in TE and TM mode, respectively. Not only the RF–DC conversion, the power management function is examined as well. Due to the cells are parallelly linked, the harvester, which can be considered equal to a DC voltage source, yields a small intrinsic resistance. That property is beneficial, it enables the fast charging of the intermediate capacitor and thus quickly obtain the usable output voltage. Not only that, the proposed harvester, with a simple DC combining method, can be easily modified to incorporate more unit cells into it, thus harvests more power and further reduce the charging time. With such advantages, the harvester of this works is suitable and potential to be used in real life applications.

ACKNOWLEDGMENT

The authors thank Pham Anh Duc and Vu Hong Son for fruitful discussion and advices, RF3I lab members, VHT-Viettel Corporation and VinSmart-Vingroup for assisting in fabrication and measurement using their trial 5G products.

REFERENCES

[1] N. I. Landy, S. Sajuyigbe, J. J. Mock, D. R. Smith, and W. J. Padilla, "Perfect metamaterial absorber," *Phys. Rev. Lett.*, vol. 100, May 2008, Art. no. 207402.

[2] K. Iwaszczuk, A. C. Strikwerda, K. Fan, X. Zhang, R. D. Averitt, and P. U. Jepsen, "Flexible metamaterial absorbers for stealth applications at terahertz frequencies," *Opt. Exp.*, vol. 20, no. 1, p. 635, Jan. 2012.

[3] U. T. D. Thuy, N. T. Thuy, N. T. Tung, E. Janssens, and N. Q. Liem, "Large-area cost-effective lithography-free infrared metasurface absorbers for molecular detection," *APL Mater.*, vol. 7, no. 7, Jul. 2019, Art. no. 071102.

[4] *NRF52811 Datasheet*, Nordic Semiconductor, Trondheim, Norway, Feb. 2019.

[5] *CC2650 SimpleLink TM Multistandard Wireless MCU*, Texes Instruments, Dallas, TX, USA, Feb. 2015.

[6] M. Pinuela, P. D. Mitcheson, and S. Lucyszyn, "Ambient RF energy harvesting in urban and semi-urban environments," *IEEE Trans. Microw. Theory Techn.*, vol. 61, no. 7, pp. 2715–2726, Jul. 2013.

[7] M. Cansiz, D. Altinel, and G. K. Kurt, "Efficiency in RF energy harvesting systems: A comprehensive review," *Energy*, vol. 174, pp. 292–309, May 2019.

[8] T. S. Almoneef and O. M. Ramahi, "Metamaterial electromagnetic energy harvester with near unity efficiency," *Appl. Phys. Lett.*, vol. 106, no. 15, 2015, Art. no. 153902.

[9] S. Shang, S. Yang, M. Shan, J. Liu, and H. Cao, "High performance metamaterial device with enhanced electromagnetic energy harvesting efficiency," *AIP Adv.*, vol. 7, no. 10, Oct. 2017, Art. no. 105204.

[10] A. Ghaneizadeh, K. Mafinezhad, and M. Joodaki, "Design and fabrication of a 2D-isotropic flexible ultra-thin metasurface for ambient electromagnetic energy harvesting," *AIP Adv.*, vol. 9, no. 2, Feb. 2019, Art. no. 025304.

[11] T. S. Almoneef, F. Erkmen, and O. M. Ramahi, "Harvesting the energy of multi-polarized electromagnetic waves," *Sci. Rep.*, vol. 7, no. 1, Nov. 2017, Art. no. 14656.

[12] A. Z. Ashoor and O. M. Ramahi, "Polarization-independent cross-dipole energy harvesting surface," *IEEE Trans. Microw. Theory Techn.*, vol. 67, no. 3, pp. 1130–1137, Mar. 2019.

[13] J. Zhou, E. N. Economon, T. Koschny, and C. M. Soukoulis, "Unifying approach to left-handed material design," *Opt. Lett.*, vol. 31, no. 24, p. 3620, Dec. 2006.

[14] Y. Zhang, T. Li, Q. Chen, H. Zhang, J. F. O'Hara, E. Abele, A. J. Taylor, H.-T. Chen, and A. K. Azad, "Independently tunable dual-band perfect absorber based on graphene at mid-infrared frequencies," *Sci. Rep.*, vol. 5, no. 1, Nov. 2016, Art. no. 18463.

[15] Y. Cheng, R. Gong, and J. Zhao, "A photoexcited switchable perfect metamaterial absorber/reflector with polarization-independent and wide-angle for terahertz waves," *Opt. Mater.*, vol. 62, pp. 28–33, Dec. 2016.

[16] X. Chen, T. M. Grzegorczyk, B.-I. Wu, J. Pacheco, Jr., and J. A. Kong, "Robust method to retrieve the constitutive effective parameters of metamaterials," *Phys. Rev. E, Stat. Phys. Plasmas Fluids Relat. Interdiscip. Top.*, vol. 70, no. 1, 2004, Art. no. 016608.

[17] S. Hemour, Y. Zhao, C. H. P. Lorenz, D. Houssameddine, Y. Gui, and C.-M. Hu, "Towards low-power high-efficiency RF and microwave energy harvesting," *IEEE Trans. Microw. Theory Techn.*, vol. 62, no. 4, pp. 965–976, Apr. 2014.

[18] H. Sun, Y.-X. Guo, M. He, and Z. Zhong, "A dual-band rectenna using broadband Yagi antenna array for ambient RF power harvesting," *IEEE Antennas Wireless Propag. Lett.*, vol. 12, pp. 918–921, 2013.

[19] T. Matsunaga, E. Nishiyama, and I. Toyada, "5.8-GHz stacked differential rectenna suitable for large-scale rectenna arrays with DC connection," *IEEE Trans. Antennas Propag.*, vol. 63, no. 12, pp. 5944–5949, Dec. 2015.

[20] H. Sun and W. Geyi, "A new rectenna using beamwidth-enhanced antenna array for RF power harvesting applications," *IEEE Antennas Wireless Propag. Lett.*, vol. 16, pp. 1451–1454, 2017.

[21] M. El Badawe, T. S. Almoneef, and O. M. Ramahi, "A metasurface for conversion of electromagnetic radiation to DC," *AIP Adv.*, vol. 7, no. 3, 2017, Art. no. 035112.

[22] A. Mavaddat, S. H. M. Armaki, and A. R. Erfanian, "Millimeter-wave energy harvesting using 4×4 microstrip patch antenna array," *IEEE IEEE Antennas Wireless Propag. Lett.*, vol. 14, pp. 515–518, 2015.

[23] A. Z. Ashoor, T. S. Almoneef, and O. M. Ramahi, "A planar dipole array surface for electromagnetic energy harvesting and wireless power transfer," *IEEE Trans. Microw. Theory Techn.*, vol. 66, no. 3, pp. 1553–1560, Mar. 2018.

[24] Q. Awais, Y. Jin, H. T. Chattha, M. Jamil, H. Qiang, and B. A. Khawaja, "A compact rectenna system with high conversion efficiency for wireless energy harvesting," *IEEE Access*, vol. 6, pp. 35857–35866, 2018.

[25] A. C. Torres, "GSM Cell Broadcast Service security analysis," M.S. thesis, Dept. Math. Comput. Sci., Eindhoven Univ. Technol., Eindhoven, The Netherlands, Aug. 2013.

[26] A. M. Hawkes, A. R. Katko, and S. A. Cummer, "A microwave metamaterial with integrated power harvesting functionality," *Appl. Phys. Lett.*, vol. 103, Oct. 2013, Art. no. 163901.

[27] X. Duan, X. Chen, and L. Zhou, "A metamaterial electromagnetic energy rectifying surface with high harvesting efficiency," *AIP Adv.*, vol. 6, Dec. 2016, Art. no. 125020.

MINH DINH (Member, IEEE) received the Diploma degree in electrical engineering from Hanoi University of Science and Technology, in 2021. He is currently working on metamaterials and other microwave periodic structures.

NAM HA-VAN (Member, IEEE) received the B.S. degree from the School of Electronics and Telecommunications, Hanoi University of Science and Technology, Hanoi, Vietnam, in 2012, and the Ph.D. degree in information and telecommunication engineering from Soongsil University, Seoul, South Korea, in February 2019. He was a Postdoctoral Researcher with Soongsil University from March 2019 to September 2020. He is currently a Postdoctoral Researcher with the Department of Electronics and Nanoengineering, School of Electrical Engineering, Aalto University, Finland. His research interests include wireless power transfer, metamaterials, antennas, and energy harvesting systems.

NGUYEN THANH TUNG (Member, IEEE) received the B.E. degree in applied physics from Hanoi University of Science and Technology, in December 2009, the M.Sc. degree from the Department of Physics, Hanyang University, Seoul, South Korea, and the Ph.D. degree from the Department of Physics and Astronomy, Katholieke Universiteit Leuven, in 2014. In August 2015, he has joined the Metamaterials Laboratory of Prof. Takuo Tanaka, RIKEN, Wako, Japan, as a Japan Society for Promotion of Science (JSPS) Postdoctoral Fellow. He previously worked on the field of optics, magnetism, and spectroscopic characterizations. His works focused on fundamentals and applications of artificially engineered materials, in one hand, from top-down such as electromagnetic metamaterials, and in the other hand, from bottom-up such as multi-element atomic clusters, including simulations and measurements of microwave, infrared, and optical structures, especially the physics of magnetic materials at the atomic level using the Stern-Gerlach magnetic deflection technique. He is currently working as the Principal Researcher of the Institute of Materials Science (IMS) and an Associate Professor at the Graduate University of Science and Technology (GUST), Vietnam Academy of Science and Technology (VAST). His research interest includes to investigate the use of thermal plasma technology to massively produce nanomaterials for real applications.

MINH THUY LE (Member, IEEE) was born in Vietnam. She received the degree in engineering and the M.S. degree in electrical engineering from Hanoi University of Science and Technology, in 2006 and 2008, respectively, and the Ph.D. degree in optics and radio frequency from Grenoble Institute of Technology, France, in 2013. She is a Lecturer and also the Group Leader of Radio Frequency Group at the Department of Instrumentation and Industrial Informatics (3I), School of Electrical Engineering (SEE), Hanoi University of Science and Technology (HUST). Her current research interests include built-in antenna, antenna array, beamforming, metamaterials, indoor localization and RF energy harvesting, wireless power transfer, and autonomous wireless sensor.